Large scale observations and strain partitioning analysis in Guatemala from SAR interferometry

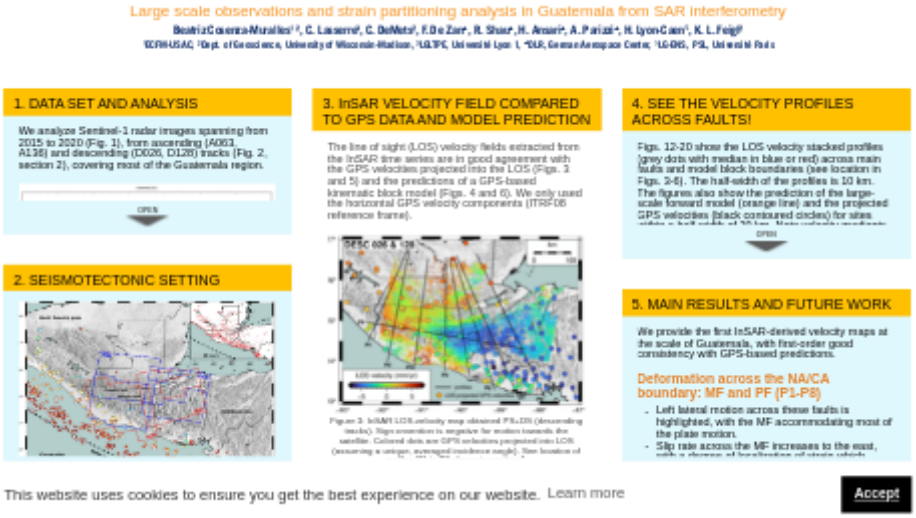

Beatriz Cosenza-Muralles[1] [2], C. Lasserre[3], C. DeMets[2], F. De Zan[4], R. Shau[4], H. Ansari[4], A. Parizzi[4], H. Lyon-Caen[5], K. L. Feigl[2]

[1]ECFM-USAC, [2]Dept. of Geoscience, University of Wisconsin-Madison, [3]LGLTPE, Université Lyon 1, [4]DLR, German Aerospace Center, [5]LG-ENS, PSL, Université Paris

PRESENTED AT:

1. DATA SET AND ANALYSIS

We analyze Sentinel-1 radar images spanning from 2015 to 2020 (Fig. 1), from ascending (A063, A136) and descending (D026, D128) tracks (Fig. 2, section 2), covering most of the Guatemala region.

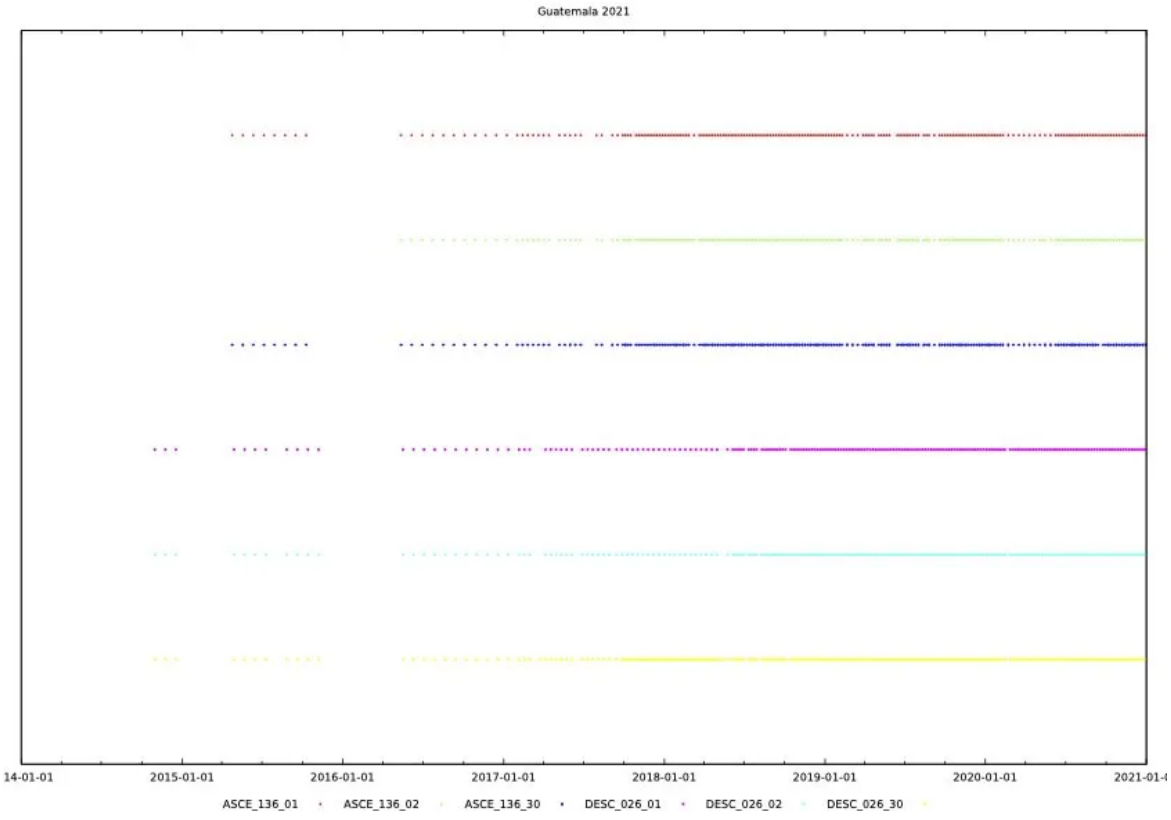

Figure 1: Time coverage of the Sentinel-1 data set.

PERSISTENT SCATTERER (PS) + DISTRIBUTED SCATTERER (DS) INTERFEROMETRY

We use Distributed Scatterers (DS) Interferometry techniques adapted to large Sentinel-1 data sets to better assess and mitigate the various sources of noise (Ansari et al. 2018; De Zan et al. 2015).

Main difficulties:

- Connecting clusters of points is challenging due to strong tropospheric phase delays and distance between clusters.

Approach:

- Wide area persistent scatterer interferometry using the DSL IWAP-PSI processor (Adam et al. 2013).
- Distributed scatterer (DS) interferometry with efficient phase estimation for interferogram stacks using the EMI algorithm developed by Ansari et al.

(2018) (phase estimated using the full temporal covariance matrix).

- Large scale tropospheric mitigation performed using the ERA-5 ECMWF reanalysis data set (Xiaoying et al. 2018; Parizzi et al. 2020).
- Ionosphere corrections performed with GNSS-based models (CODE).

2. SEISMOTECTONIC SETTING

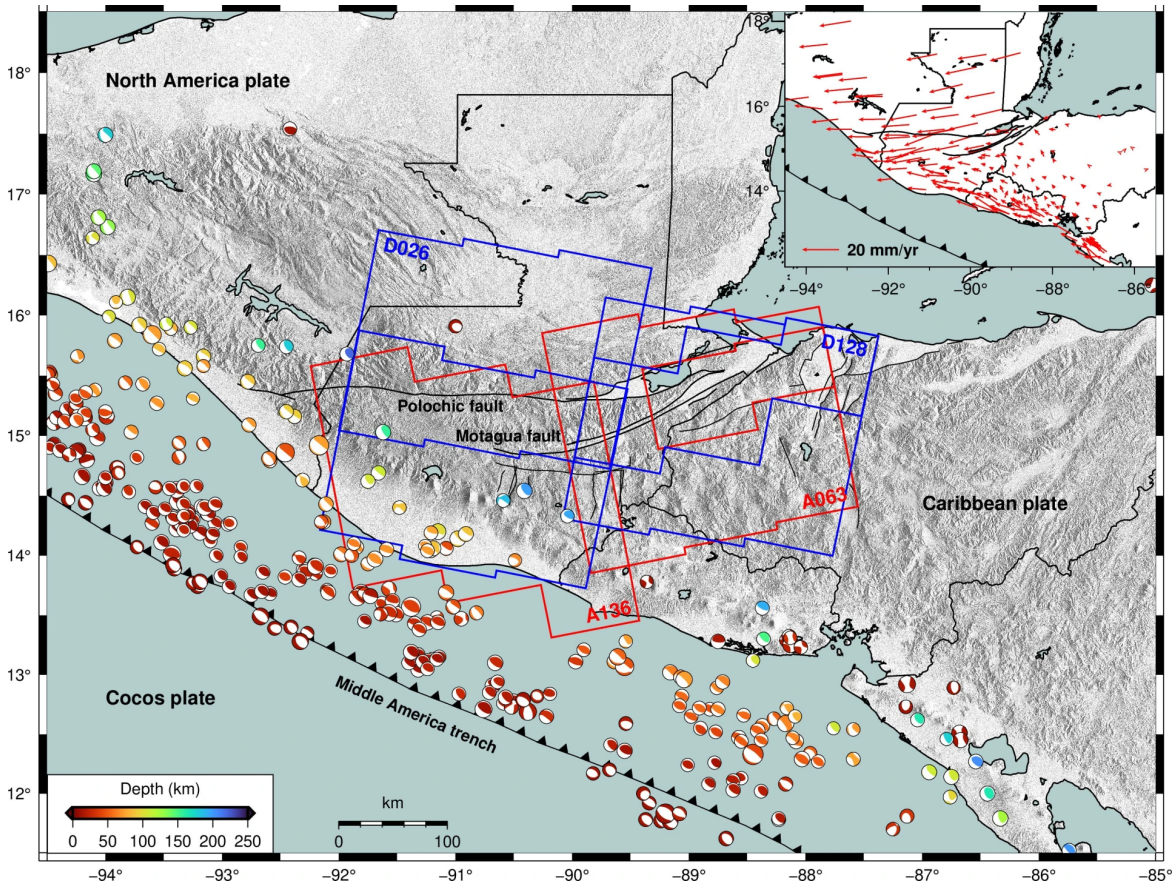

Figure. 2: Regional seismotectonic setting. Seismicity from Oct 2014 to Dec 2020 (Global CMT catalog). Boxes show the location the ascending (red) and descending (blue) Sentinel 1 tracks analyzed in this study. Inset shows the GPS velocity field (Caribbean plate reference frame) from Ellis et al. (2018).

The interaction between the Cocos (CO), Caribbean (CA), and North America (NA) plates in Central America results in complex deformation mostly accommodated by the sub-parallel Motagua (MF) and Polochic (PF) left-lateral faults, north-south-trending extensional grabens south of the MF, the Middle America subduction zone, and right-lateral faults along the Middle America volcanic arc. Large earthquakes associated with these faults include the destructive 1976 Mw 7.5 earthquake along the MF and the 2012 Mw 7.5 Champerico subduction thrust earthquake. The latest published GPS-based present-day kinematic model of the region (Ellis et al. 2019) shows that about 80% of the strain accumulation from the North America/Caribbean plates relative motion concentrates on the Motagua fault and 20% across the Polochic fault, with significant internal stretching of the Caribbean plate between Honduras and western Guatemala, a decreasing strike-slip rate from east to west along the volcanic arc, and lateral variations of coupling along the subduction zone.

We propose to use interferometric synthetic aperture radar (InSAR) data to measure strain rates across faults in Guatemala and constrain slip partitioning among the different faults.

3. INSAR VELOCITY FIELD COMPARED TO GPS DATA AND MODEL PREDICTION

The line of sight (LOS) velocity fields extracted from the InSAR time series are in good agreement with the GPS velocities projected into the LOS (Figs. 3 and 5) and the predictions of a GPS-based kinematic block model (Figs. 4 and 6). We only used the horizontal GPS velocity components (ITRF08 reference frame).

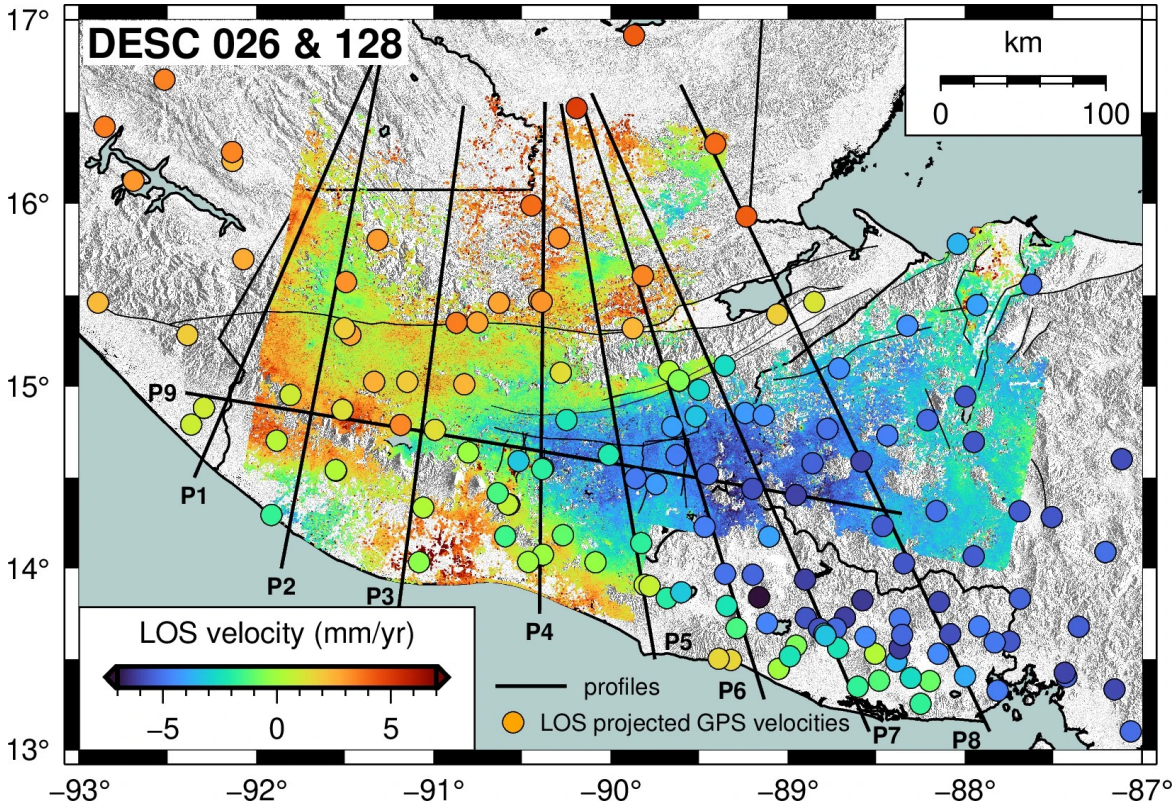

Figure 3: InSAR LOS-velocity map obtained PS+DS (descending tracks). Sign onvention is negative for motion towards the satellite. Colored dots are GPS velocities projected into LOS (assuming a unique, averaged incidence angle). See location of profiles P1 to P9 shown in section 4.

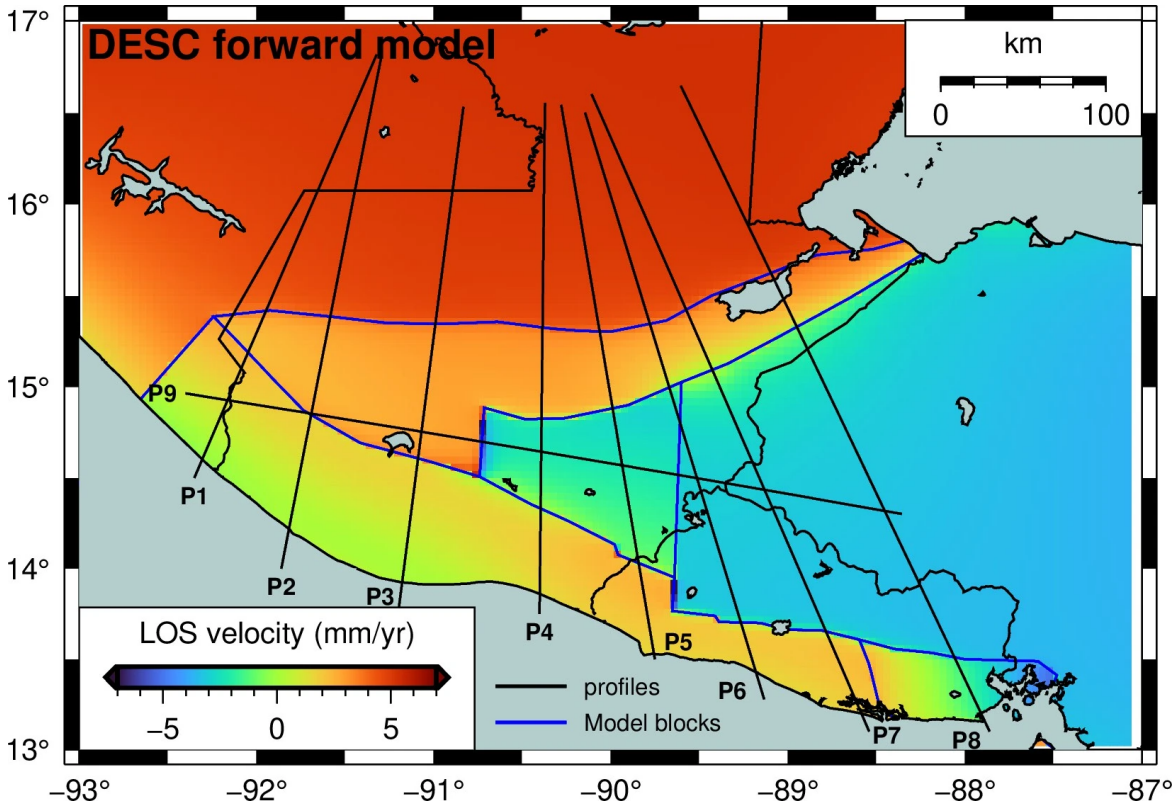

Figure 4: Predicted LOS velocities (descending tracks) for a forward model, based on the best-fitting estimates of interseismic locking for faults and relative block motion along the Central America volcanic arc, the MF and PF, the main grabens, and the Middle America trench, from GPS (Ellis et al., 2019). This model was generated with TDEFNODE (McCaffrey, 2009), using constant values for the incidence and heading angles as a first, large-scale approximation.

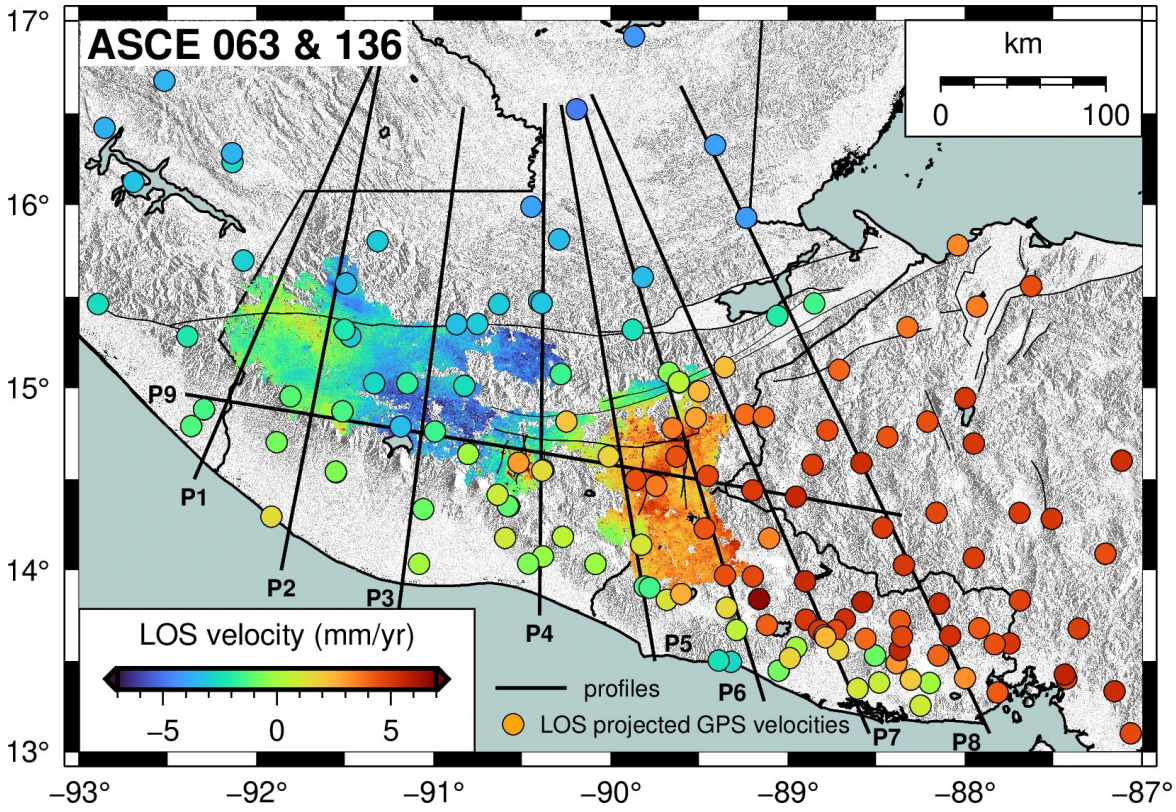

Figure 5: InSAR LOS-velocity map obtained PS+DS (ascending tracks). Sign onvention is negative for motion towards the satellite. Colored dots are GPS velocities projected into LOS (assuming a unique, averaged incidence angle). See location of profiles P1 to P9 shown in section 4.

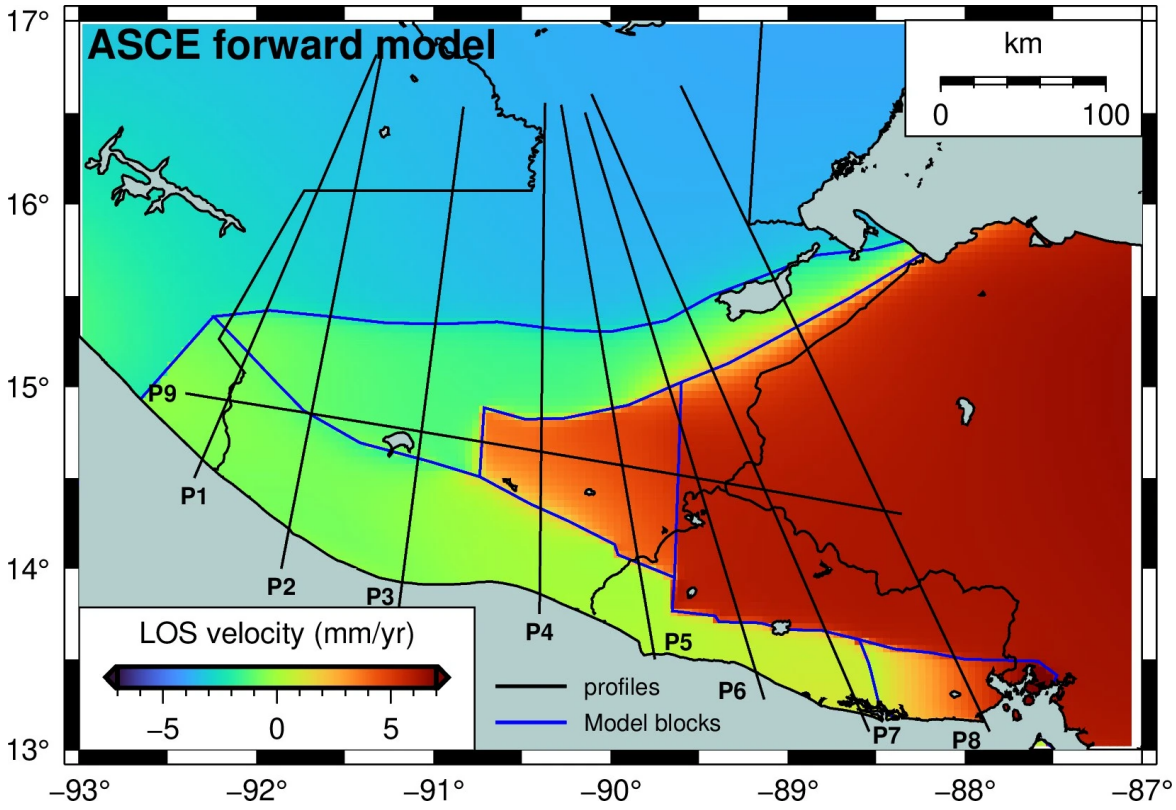

Figure 6: Predicted LOS velocities (ascending tracks) for a forward model, based on the best-fitting estimates of interseismic locking for faults and relative block motion along the Central America volcanic arc, the MF and PF, the main grabens, and the Middle America trench, from GPS (Ellis et al., 2019). This model was generated with TDEFNODE (McCaffrey, 2009), using constant values for the incidence and heading angles as a first, large-scale approximation.

We also produced forward models for each separate track and using the LOS vector at each position. Figs 7-11 show a comparison between the InSAR LOS velocities and the models.

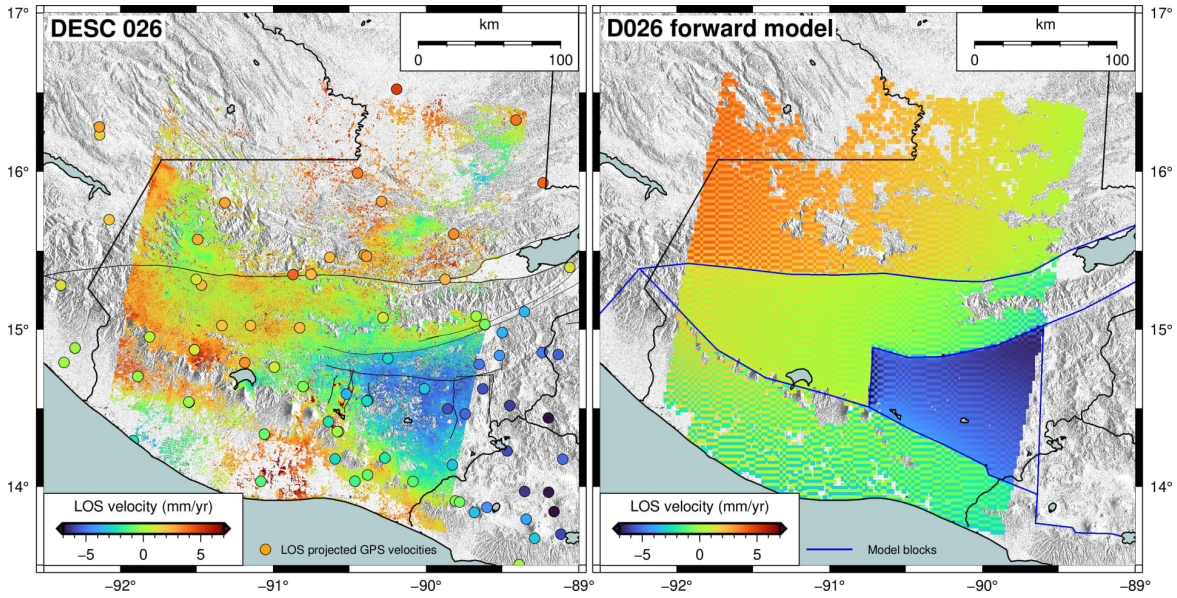

Figure 7: Left: InSAR LOS velocities for track D026. Right: LOS velocities predictions from the forward model for track D026.

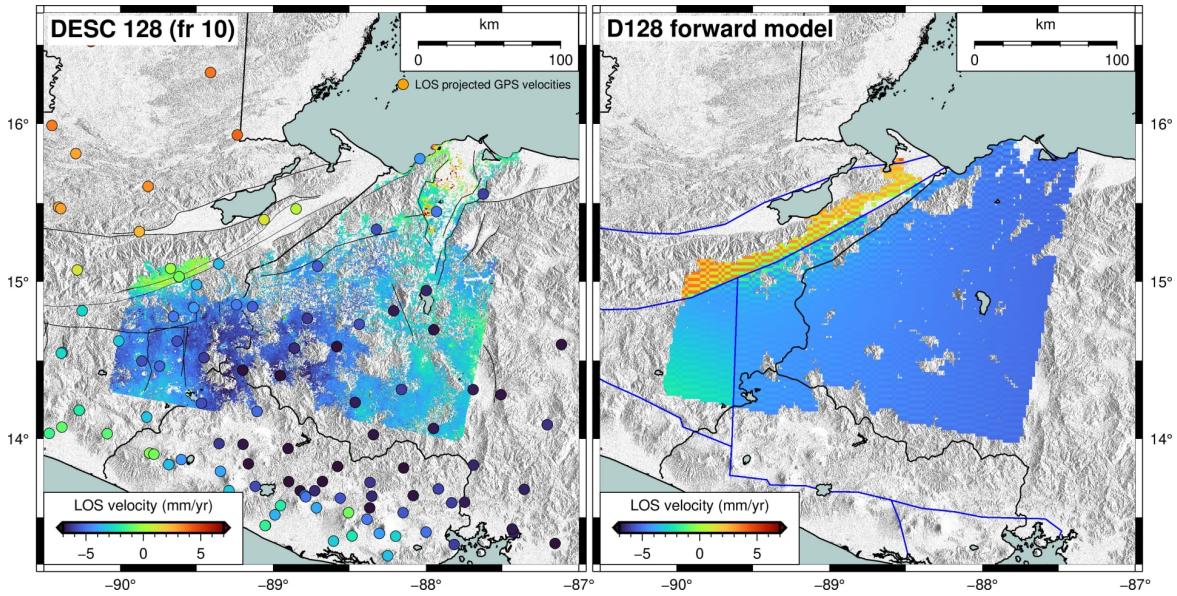

Figure 8: Left: InSAR LOS velocities for track D128, frame 10. Right: LOS velocities predictions from the forward model for track D128, frame 10.

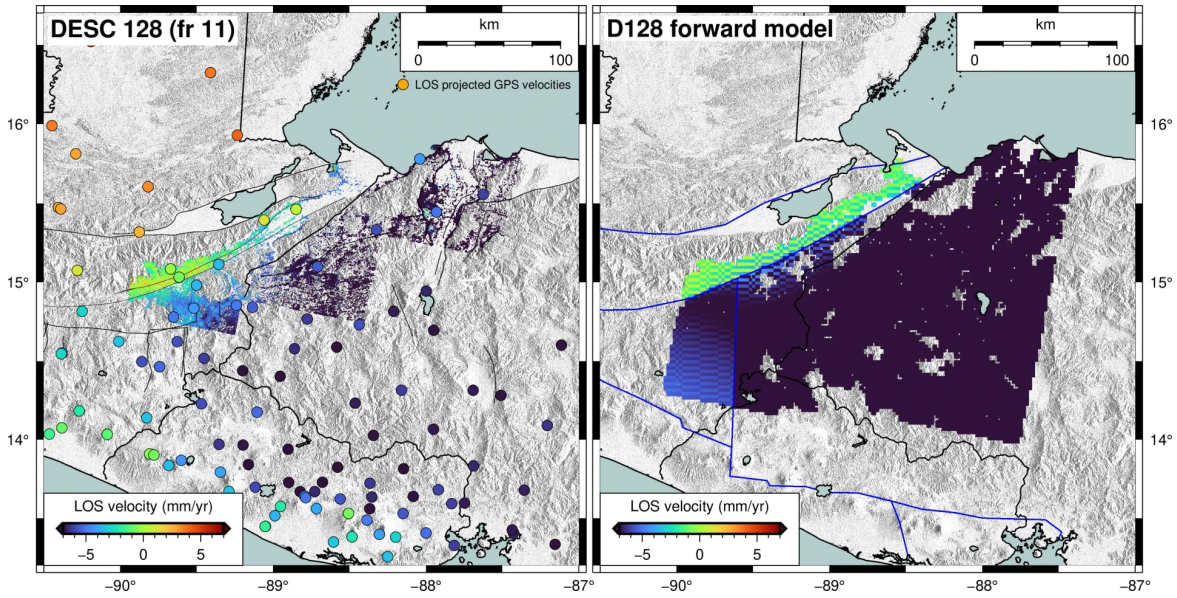

Figure 9: Left: InSAR LOS velocities for track D128, frame 11. Right: LOS velocities predictions from the forward model for track 128, frame 11.

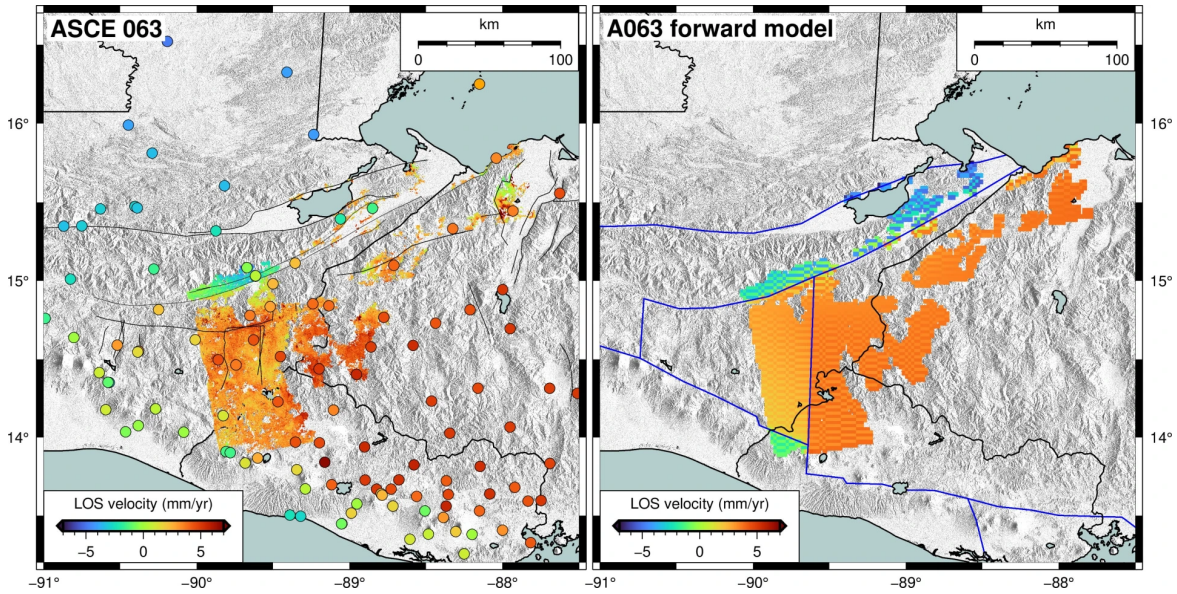

Figure 10: Left: InSAR LOS velocities for track A063. Right: LOS velocities predictions from the forward model for track A063.

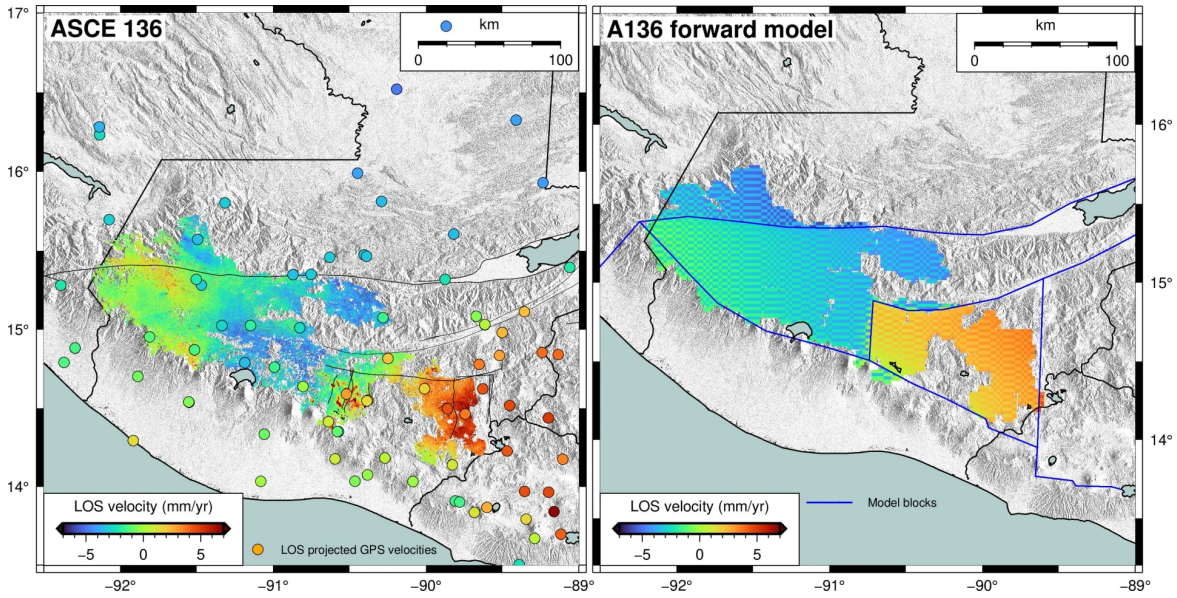

Figure 11: Left: InSAR LOS velocities for track A136. Right: LOS velocities predictions from the forward model for track A136.

4. SEE THE VELOCITY PROFILES ACROSS FAULTS!

Figs. 12-20 show the LOS velocity stacked profiles (grey dots with median in blue or red) across main faults and model block boundaries (see location in Figs. 3-6). The half-width of the profiles is 10 km. The figures also show the prediction of the large-scale forward model (orange line) and the projected GPS velocities (black contoured circles) for sites within a half-width of 20 km. Note velocity gradients across the main tectonic structures and the overall good consistency between adjacent tracks when overlapping (profiles 5-6 on descending tracks in Figs. 13 and 14), although InSAR will help refine strain localization.

Strike-slip motion in central Guatemala

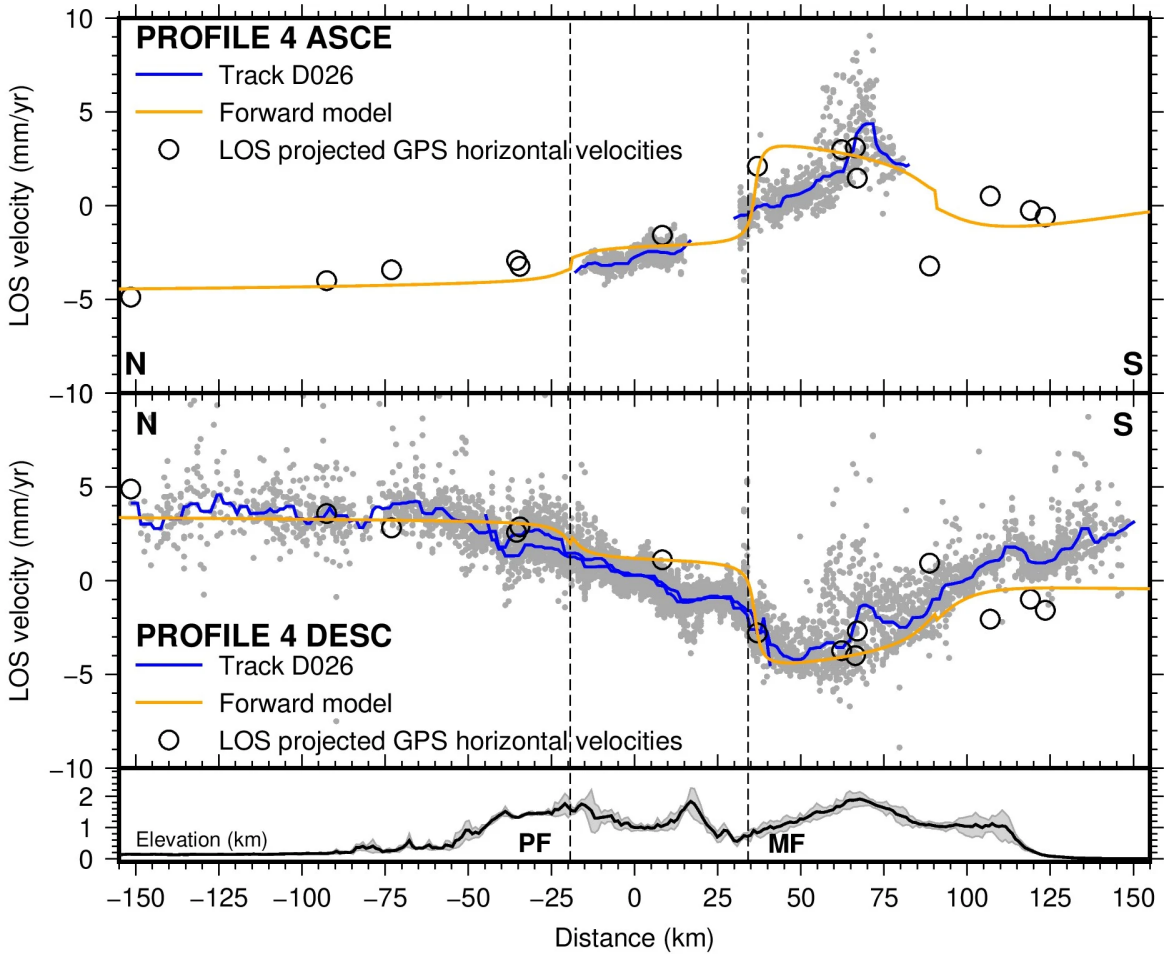

Figure 12: Profile 4.

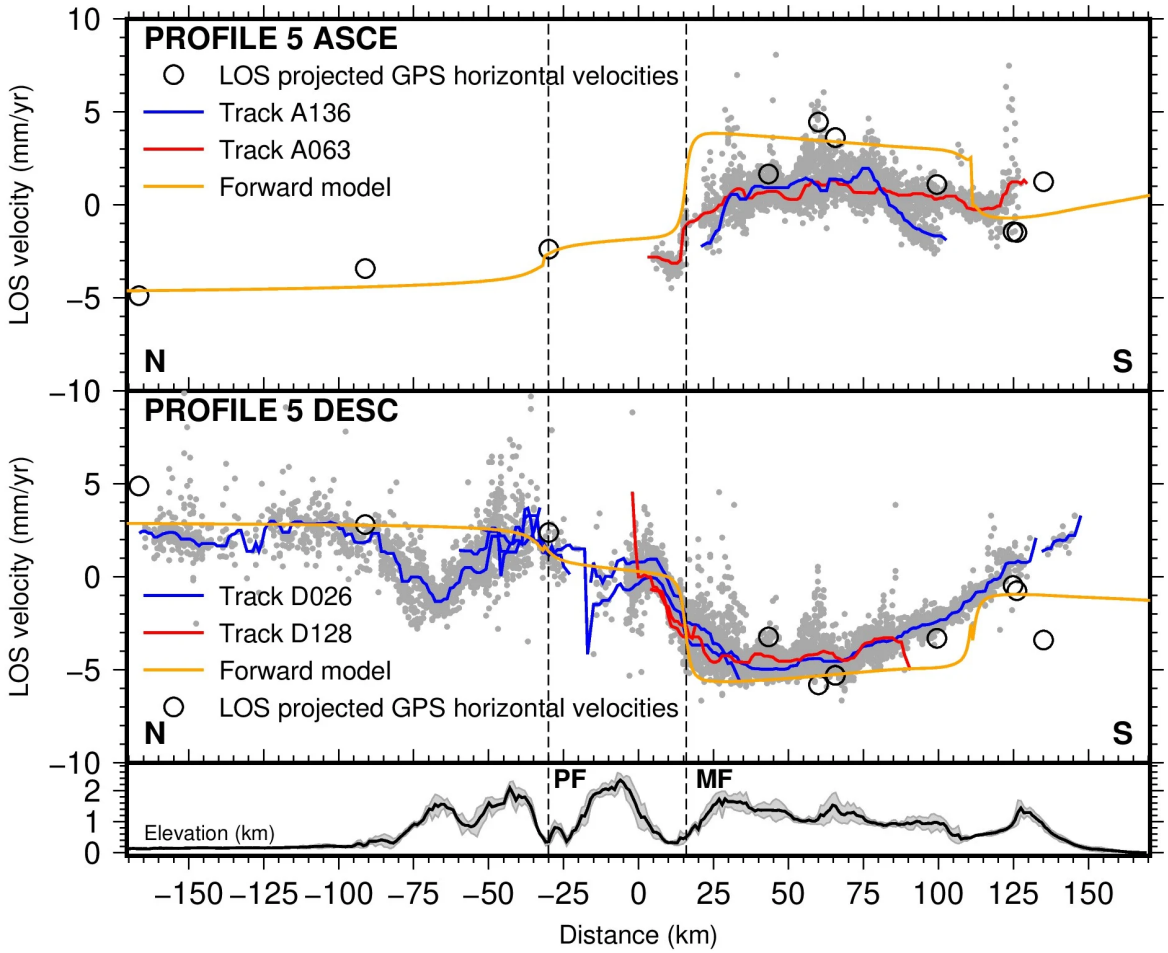

Figure 13: Profile 5

Strike-slip motion in eastern Guatemala

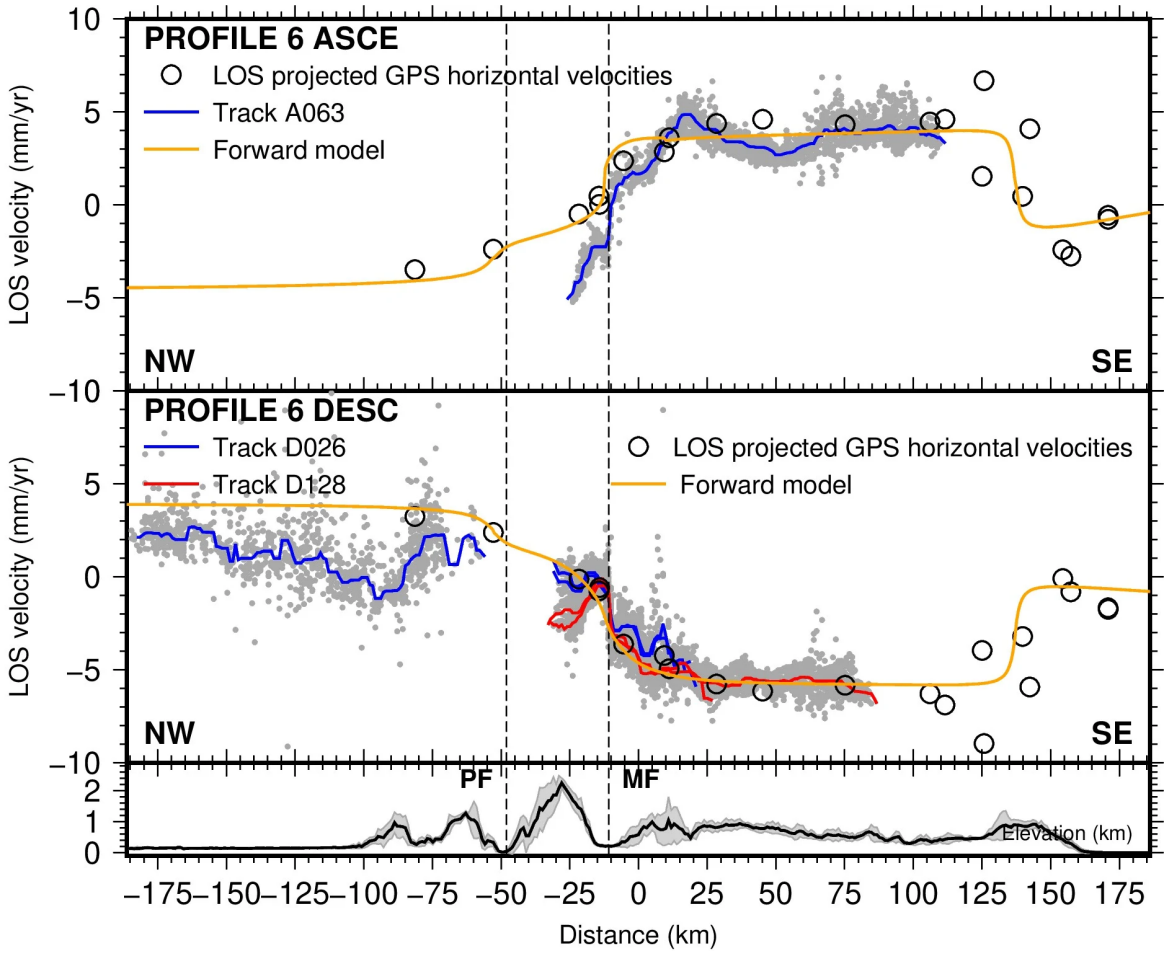

Figure 14: Profile 6

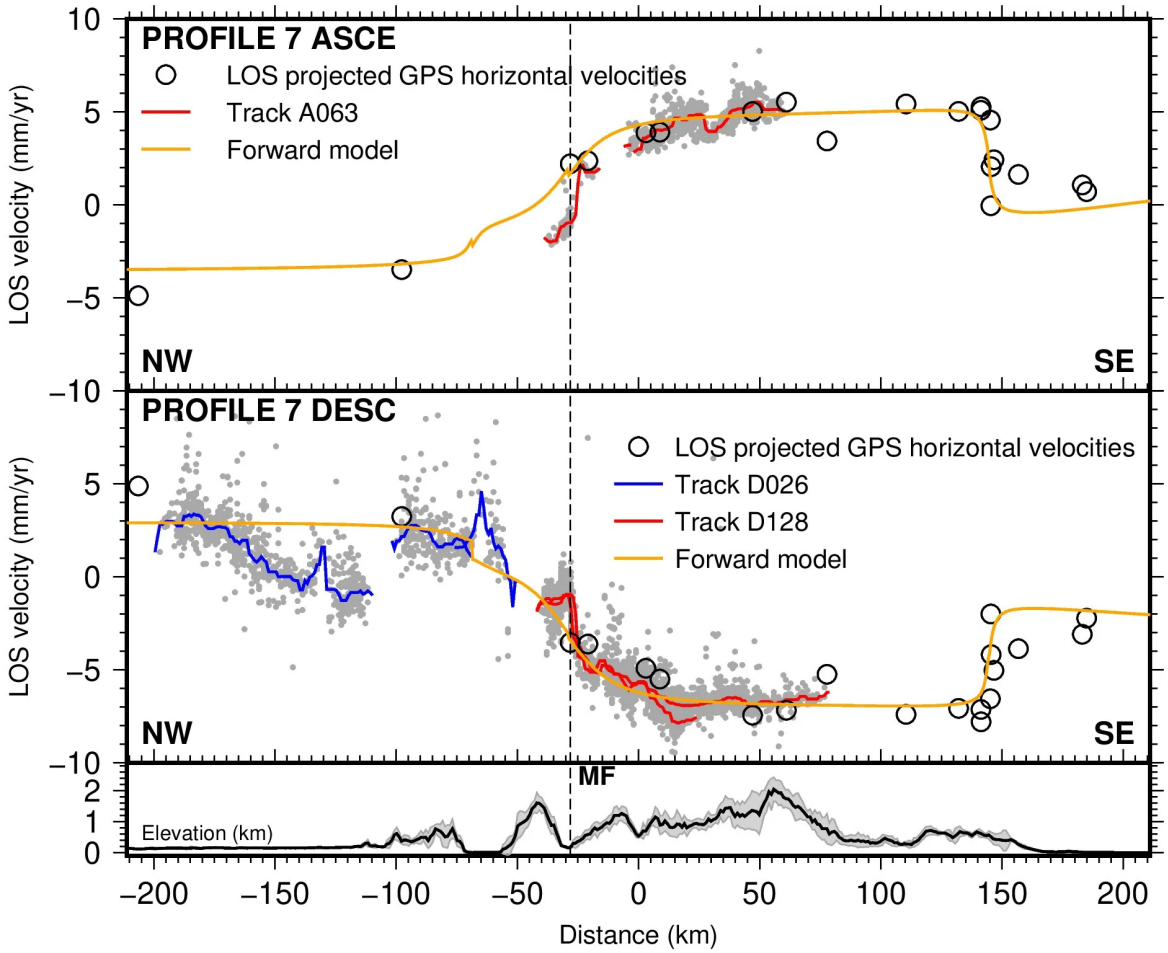

Figure 15: Profile 7.

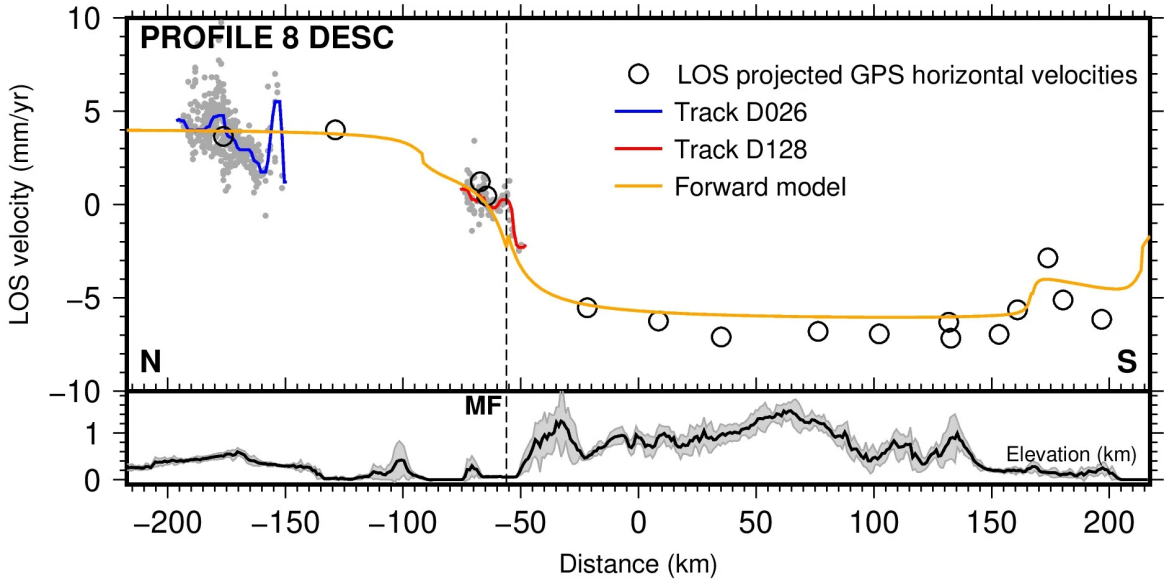

Figure 16: Profile 8.

Strike-slip motion and subduction coupling in western Guatemala

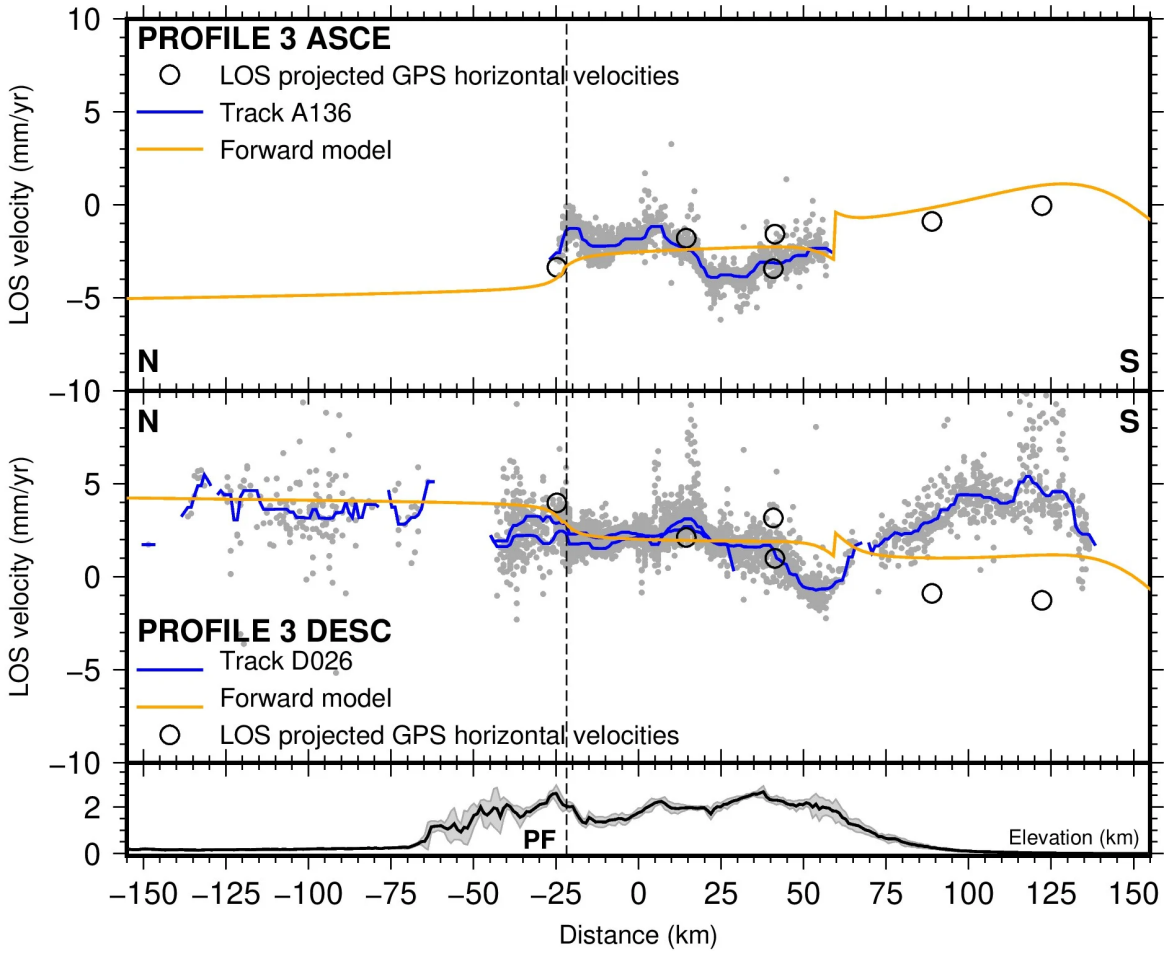

Figure 17: Profile 3.

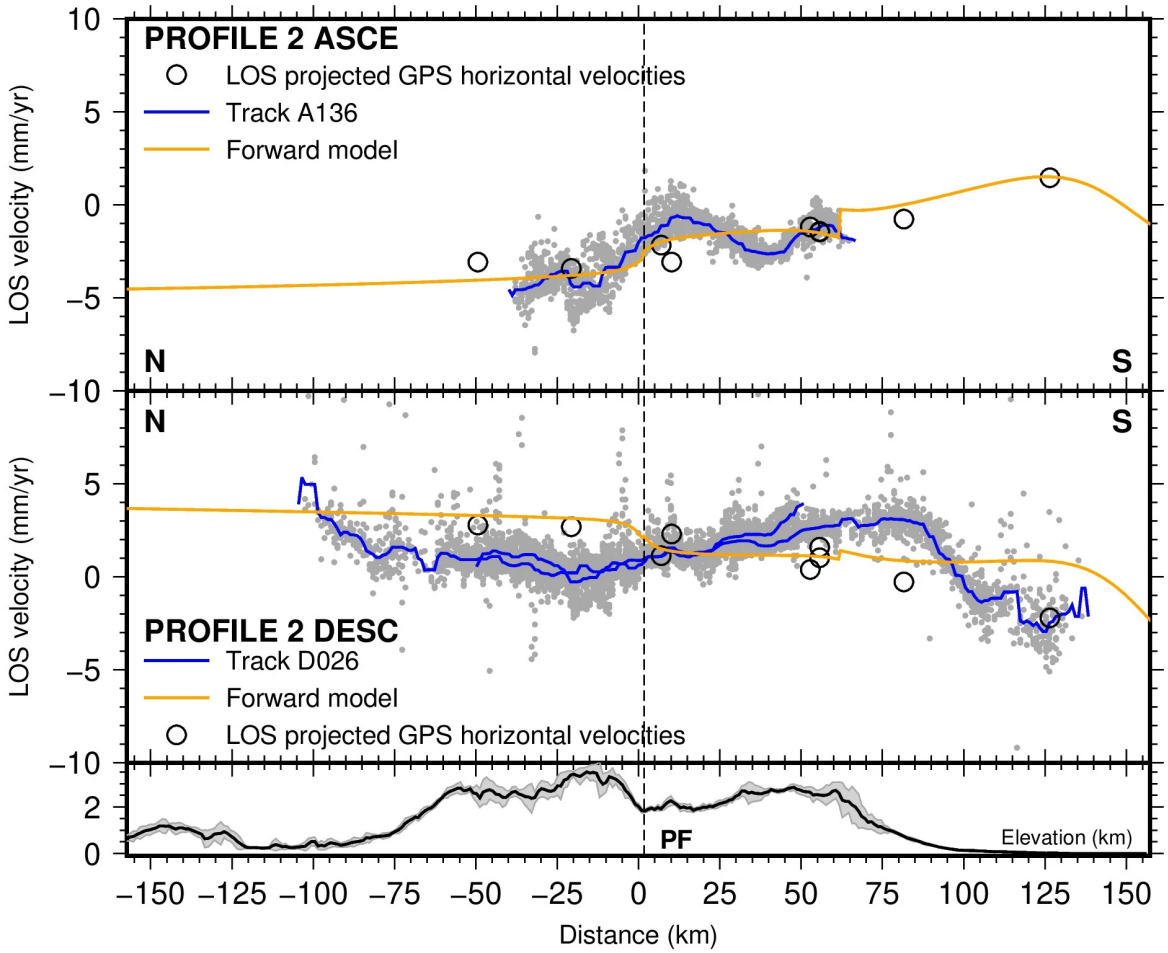

Figure 18: Profile 2.

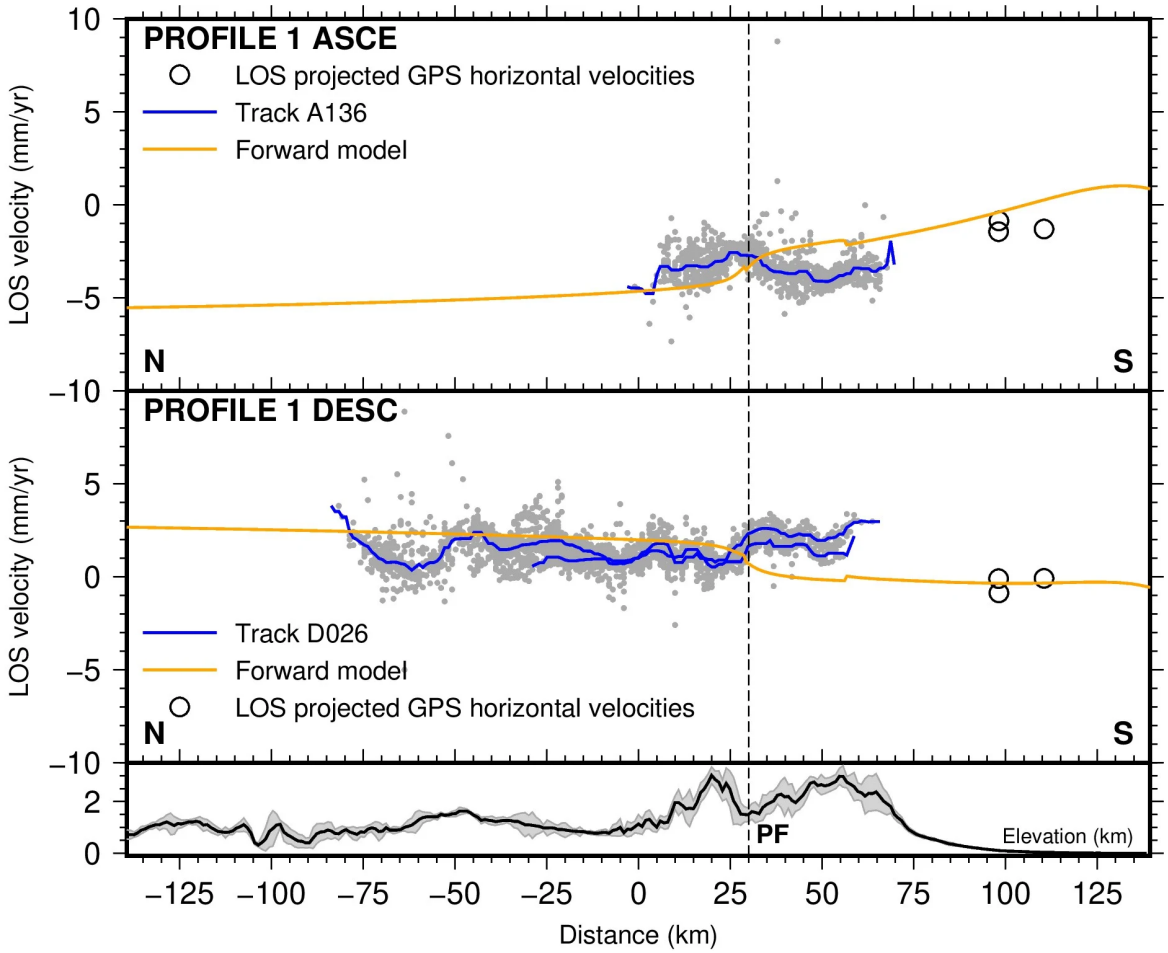

Figure 19: Profile 1.

Internal extension across Caribbean plate

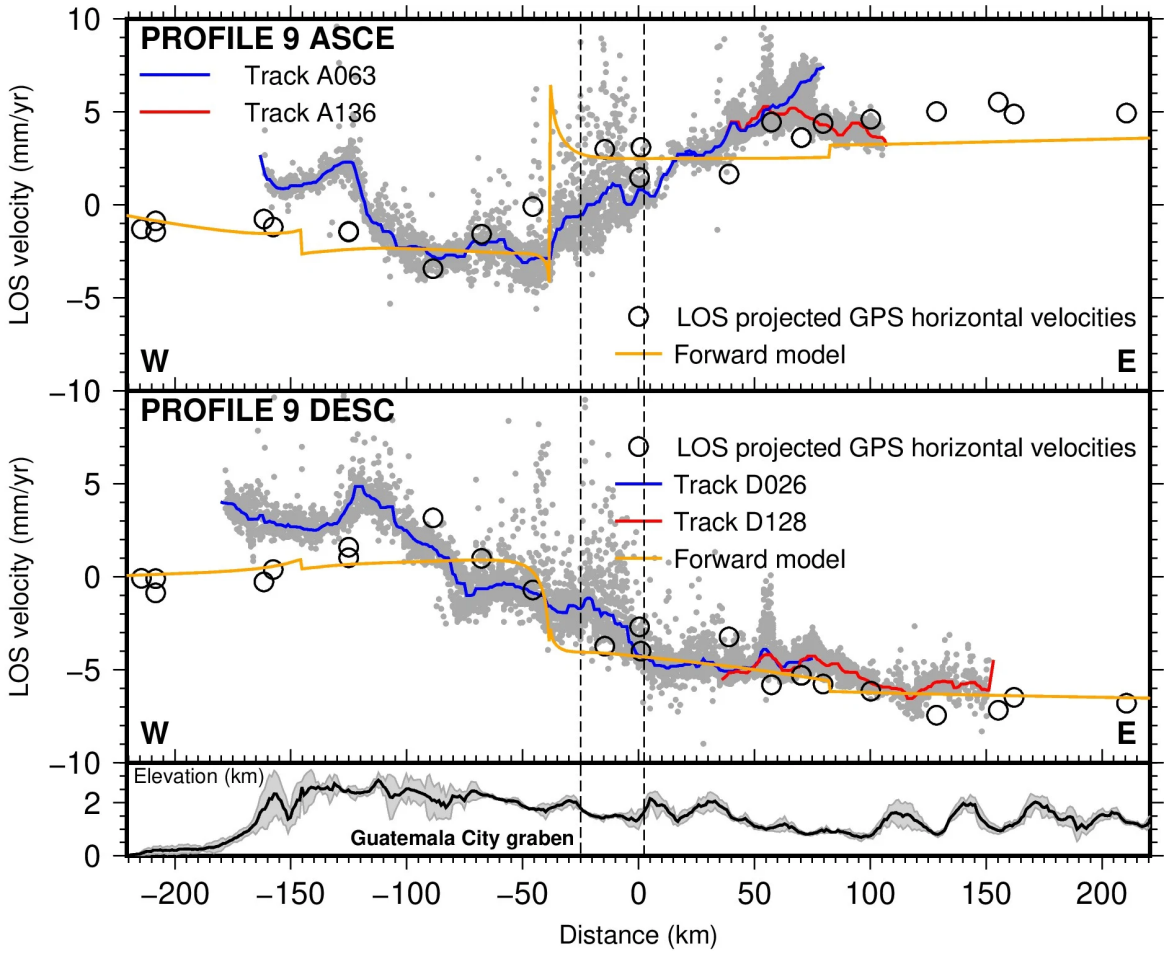

Figure 20: Profile 9.

5. MAIN RESULTS AND FUTURE WORK

We provide the first InSAR-derived velocity maps at the scale of Guatemala, with first-order good consistency with GPS-based predictions.

Deformation across the NA/CA boundary: MF and PF (P1-P8)

- Left lateral motion across these faults is highlighted, with the MF accommodating most of the plate motion.
- Slip rate across the MF increases to the east, with a degree of localization of strain which seems to vary along the fault (P4-P8).
- Compression may be associated with the western termination of the MF (same sign for ASCE and DESC, near 25km in P3)?
- The PF accommodates almost no deformation near its westernmost end (P1).

Deformation in the south: forearc sliver and subduction (P2-P5)

- Deformation is observed in southern Guatemala, near the coast.
- Some of it corresponds to right-lateral slip associated with the northern limit of the forearc sliver parallel to the volcanic arc, decreasing from east to west.
- Negative velocity gradient is observed closer to the coast, which seems to decrease toward east, and may be related to locking variations along the subduction interface.

Deformation across the grabens (P9)

- The step-like velocity gradients along the profile highlights deformation partitioning on specific tectonic features (multiple active normal faults), which have been modeled as only two sharp north-south block boundaries in previous models.

Future work

Future work will include:

- Refined post-processing of InSAR data (taking into account seasonal signal and identifying other non tectonic processes)
- Better referencing of the InSAR data sets to GPS data
- Detailed analysis of fault coupling and slip-rate variations along fault strike (MF and subduction zone in particular)

- Horizontal and vertical deformation separation from surface data analysis
- Joint InSAR-GPS inversion and modeling
- Analysis of InSAR time series at targeted locations.

DISCLOSURES

- C.L. acknowledges financial support by the French Centre National d'Etudes Spatiales (CNES) through the TOSCA program.
- Part of this work was supported by NSF grant EAR-1144418.
- Most figures were produced using Generic Mapping Tools software (Wessel & Smith 1991).

ABSTRACT

The interaction between the Cocos, Caribbean, and North America plates in Central America results in complex deformation mostly accommodated by the sub-parallel Motagua and Polochic left-lateral faults, north-south-trending extensional grabens south of the Motagua Fault, the Middle America subduction zone, and right-lateral faults along the Middle America volcanic arc. Large earthquakes associated with these faults include the destructive 1976 Mw 7.5 earthquake along the Motagua fault and the 2012 Mw 7.5 Champerico subduction thrust earthquake. The most recent GPS-based elastic-kinematic models of the region show that about 80% of the strain accumulation from the North America/Caribbean plates relative motion concentrates on the Motagua fault and 20% across the Polochic fault, with significant internal stretching of the Caribbean plate between Honduras and western Guatemala, a decreasing strike-slip rate from east to west along the volcanic arc, and lateral variations of coupling along the subduction zone. We propose the use of Synthetic Aperture Radar Interferometry (InSAR) to measure slip rates along faults in Guatemala, strain partitioning among them and potential internal deformation within blocks. We analyze Sentinel-1 radar images spanning from 2015 to 2020, from ascending and descending tracks, covering the whole Guatemala region. We use Distributed Scatterers (DS) Interferometry techniques adapted to large Sentinel-1 data sets to better assess and mitigate the various sources of noise. We present the first InSAR-based maps of interseismic velocity for this region, analyze these InSAR results over the whole surface covered by the tracks and along key profiles across main faults for a first comparison with GPS data and the GPS-based block model. The DS results show an overall good agreement with predictions from the GPS-based block model. These InSAR results along with GPS data will be used to refine the block model and estimate the lateral variations of interseismic slip deficit rates along major faults, as well as internal deformation within the western Caribbean plate.

REFERENCES

- Adam, N. et al. (2013). Wide area persistent scatterer interferometry: Current developments, algorithms and examples, Proc. IEEEE Geosci. Remote Sens. Symp., Jul. 2013, 1857-1860.
- Ansari, H. et al. (2018). Efficient Phase Estimation for Interferogram Stacks, IEEE Transactions on Geoscience and Remote Sensing (2018), Vol. 56, No. 7, 4109-4125.
- De Zan, F., Zonno, M. , abd Lopez-Dekker P. (2015). Phase inconsistencies and multiple scattering in SAR interferometry, IEEE Transactions on Geoscience and Remote Sensing 53 (12), 6608-6616.
- Ellis, A. et al. (2018) GPS constraints on deformation in northern Central America from 1999 to 2017, Part 1 - time-dependent modelling of large regional earthquakes and their post-seismic effects, Geophys. J. Int., 214, 2177-2194, doi: 10.1093/gji/ggy249
- Ellis, A. et al. (2019) GPS constraints in deformation in northern Central America from 1999 to 2017, Part 2: Block rotations and fault slip rates, fault locking and distributed deformation, Geophys. J. Int., 218, 729-754.
- Parizzi, P., Brcic, R., and De Zan, F. (2020). InSAR Performance for Large-Scale Deformation Measurement, IEEE Transactions on Geoscience and Remote Sensing, 59(10), 8510 - 8520, 10.1109/TGRS.2020.3039006
- Wessel, P. and Smith, W.H.F. (1991). Free software helps map and display data, EOS Trans. AGU, 72(41), 445–446. doi:10.1029/90EO00319.
- Xiaoying, C. et al. (2018). Mitigation of Tropospheric Delay in SAR and InSAR using NWP data: Validation and application examples, Remote Sens., 10 (10) 1515.